Two-photon photoemission spectroscopy of TiO_2(110) surfaces modified by defects and O_2 or H_2O adsorbates

Ken Onda, Bin Li, and Hrvoje Petek*
Department of Physics and Astronomy, University of Pittsburgh, Pittsburgh, Pennsylvania 15260, USA
(Received 19 February 2004; revised manuscript received 23 April 2004; published 22 July 2004)

Two-photon photoemission (2PP) spectra of TiO_2(110) surfaces are measured for the nearly perfect surface, and surfaces modified by introduction of defects and adsorbed molecules. Defects are generated on nearly perfect surfaces by three methods: electron irradiation, annealing in vacuum, and Ar^+ sputtering. Nearly perfect or damaged surfaces can be further modified by adsorption of O_2 or H_2O molecules. 2PP spectroscopy is used to systematically investigate the work function change due to the presence of defects or adsorbates. 2PP spectroscopy detects both surface and bulk oxygen vacancy defects. We find from the results on oxygen adsorption that oxygen vacancies created by electron irradiation are localized on the surface and may be removed by O_2 adsorption at 100 K. The surface defects are substantially different from those created by annealing or by ion sputtering where vacancies in the subsurface region are proposed. We find that O_2 acts as an acceptor molecule on surface defect states whereas H_2O acts as a donor molecule. From simulation of the work function change as a function of dosage, the dipole moment of H_2O adsorbed on TiO_2 surface is derived to be 0.5 D positive outward. We also find an unoccupied electronic state 2.45 eV above the Fermi level that appears at submonolayer coverage of H_2O, which we tentatively assign to charge transfer from surface titanium ions to the surface-adsorbed H_2O molecules or OH ligands.

DOI: 10.1103/PhysRevB.70.045415 PACS number(s): 79.60.−i, 68.47.Gh, 68.43.−h, 82.65.+r

I. INTRODUCTION

Titanium dioxide (TiO_2) is a versatile material with a broad range of applications, for example, as a pigment in paints, a photocatalyst film for surface decontamination, and a photovoltaic material for solar energy conversion.[1–4] The nearly perfect rutile TiO_2(110) surface, which is simple to prepare and relatively stable, has been investigated extensively both as a representative surface of TiO_2 and more generally as a model for the chemical and electronic properties of oxide surfaces.[4] Modified TiO_2(110) surfaces, where defects are introduced in a controlled manner, are also of great interest because defect sites form reactive centers that either strongly bind or dissociate adsorbed molecules on the otherwise relatively inert oxide surface. To create defect sites on TiO_2(110) surfaces under ultrahigh vacuum conditions three simple ways are commonly used, namely, vacuum annealing, electron irradiation, and Ar^+ sputtering. Despite extensive studies, the structure and the interaction with adsorbates of these defective surfaces are not well understood.[4]

Adsorption of atmospheric molecules such as O_2 or H_2O is central to understanding the properties of TiO_2 under ambient conditions. These molecules strongly interact with TiO_2 surfaces and are thought to have central role in photocatalytic reactions and for self-cleaning properties of TiO_2 films.[3,5,6] The behavior of the oxygen molecule is complicated even on single crystalline TiO_2(110) surfaces and is not yet fully understood. For example, the adsorption site and structure of oxygen, and the dynamics when thermally or electronically excited on TiO_2 surfaces are of considerable interest because O_2 dissociation can heal oxygen vacancy defects. Furthermore, the superoxo species O_2^- formed by charge transfer from the conduction band of TiO_2 has been proposed as a reactive intermediate in the photo-oxidation of organic molecules.[4,7–9] Water adsorption on TiO_2 is also complex as evidenced by multiple peaks in temperature programmed desorption (TPD) spectra. Water molecules can adsorb on terminal Ti^{4+} sites[10] between the bridging oxygen atoms (see Fig. 1) or dissociate at oxygen vacancy defect sites to form pairs of surface hydroxyl ligands. The interaction of water with photogenerated holes is thought to produce OH radicals, which are also potent oxidizing agents of organic molecules.[11] Under atmospheric conditions, TiO_2 films are transformed from superhydrophobic to amphilic by irradiation with UV light; the origin of this transformation is not fully understood, but it underscores the complexity of the thermal and electronic interactions between H_2O and TiO_2 surfaces.[11,12]

The interaction H_2O and O_2 with the TiO_2(110) surface has been studied by many ultrahigh vacuum (UHV) surface science techniques including TPD, ultraviolet photoemission

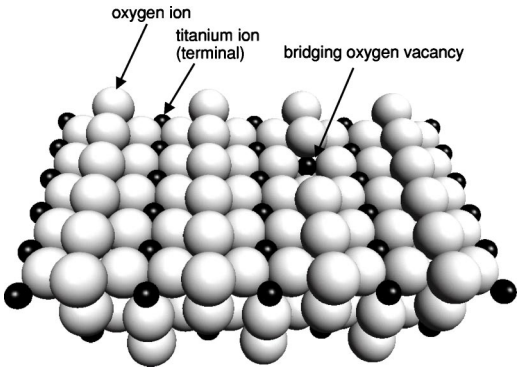

FIG. 1. Schematic structure of rutile TiO_2(110) surface. Larger spheres represent oxygen ions and smaller spheres the Ti ions. The most common bridging oxygen vacancy is also indicated.

(UPS), scanning tunneling microscopy (STM), high-resolution electron energy loss spectroscopy (HREELS), and others.[4] However, these techniques mostly probe the ground state properties of adsorbate-covered surfaces. Here we present a method for studying the electronic structure and excited state dynamics of oxide surfaces. We investigate the electronic structure of perfect, defective, and adsorbate covered TiO_2 surfaces by two-photon photoemission (2PP) spectroscopy. 2PP spectroscopy, using Ti:sapphire ultrafast laser excitation sources, has been highly successful,[13–15] for example, in the studies of structure and dynamics of image potential states on metal surface,[16,17] the hot electron dynamics in metals and semiconductors,[18,19] and the electronically excited states of atoms and molecules adsorbed on metal surfaces.[20–24] Low photon energy (1.5–6 eV) and high peak-power (Mega-Terawatt) output of ultrafast lasers enable measurement of highly sensitive photoemission spectra of ground and excited states without surface damage or desorption. However, up to now the application of 2PP to study simple metal oxide surfaces such as TiO_2 has not been reported. The 2PP spectra are very sensitive to the surface structure of TiO_2, molecular adsorption, and work function change compared with the other spectroscopic methods such as UPS. Here we report on the 2PP spectra of (1) various TiO_2 surfaces with minimum defect density, and with defects introduced by electron irradiation, vacuum annealing, and Ar^+ sputtering, and (2) the same surfaces following adsorption of oxygen and water.

II. EXPERIMENT

All experiments are carried out in an ultrahigh vacuum (UHV) system (base pressure $<1\times10^{-10}$ mbar). Before 2PP measurements, the single-crystal rutile $TiO_2(110)$ samples (Princeton Scientific, Corp.) are treated by annealing in vacuum at 1000 K for 4 h, whereby the crystals acquire a light blue color. The annealing procedure creates oxygen vacancies in the bulk introducing *n*-type doping, which is necessary to avoid the charging of the crystal during the photoemission measurements.[4]

Before each measurement the surface with minimum defects is prepared by cyclical: (1) 1000 eV Ar ion sputtering ($2\ \mu A/cm^2$) for 10 min, (2) annealing at 900 K in an atmosphere of 3×10^{-7} mbar O_2 for 40 min, and (3) final cooling to room temperature in the same O_2 atmosphere. We confirmed the surface composition and the formation of an ordered $(110)(1\times1)$ structure by Auger electron spectroscopy and low-energy electron diffraction (LEED). The quality of the surface can also be judged by the work function observed in 2PP spectra: high work function correlates with the minimum defect density. Since it is thermodynamically impossible to form a surface without some oxygen vacancies, we refer to surfaces formed by the above procedure as "nearly perfect."

All defective surfaces are prepared from the nearly perfect surface after the above preparation procedure in order to insure the best reproducibility of experimental results. The "annealed surface" is prepared by heating the nearly perfect surface at 900–1000 K in vacuum for 10–30 min. The "electron-irradiated" and "Ar^+ sputtered" surfaces are made by irradiating the nearly perfect surface with an electron gun (OMICRON NGE52; 200 nA/cm^2, 10–60 min, 500 eV) and an ion gun (OMICRON ISE10; $2\ \mu A/cm^2$, 5–20 min, 1000 eV), respectively. The sample is always cooled down to 100 K with liquid nitrogen during the molecular adsorption and 2PP measurements. Dosage of gases is carried out by the back filling method through a variable leak valve. Oxygen gas (99.998%, Matheson Tri-Gas, Inc.) is used without further purification; distilled water (H_2O) is purified by several freeze-pump and thaw cycles before adsorption.

Photoemission is measured with a hemispherical electron energy analyzer (OMICRON EA 125). A bias of 5 V is applied to the sample and only photoemission normal to the surface is collected. The observed spectra do not show dispersion, so the distortion of spectra introduced by the bias is negligible. The 2PP signal from the nearly perfect TiO_2 is weak with typical count rates of 100–5000 counts/s. The energy with respect to the Fermi level is calibrated by measuring the work function of clean and ordered Cu(111) and Ag(111) surfaces, whose work functions are well known. The upper limit of resolution of 20 meV is estimated from the sharp work function edge of photoemission.

The excitation source is a self-made Ti:sapphire oscillator using negative dispersion mirrors for dispersion compensation. The laser provides 750 mW output at 800 nm with a pulse width of 8 fs and repetition rate of 90 MHz. The laser light is converted to its second harmonic (3.05 eV photon energy; 0.2 eV spectral width) in an 80 μm BBO crystal. Before entering the chamber, the excitation pulse dispersion is precompensated with negative dispersion mirrors in order to minimize the pulse width at the sample. The laser power just before the UHV chamber is 20–50 mW. Polarization of the excitation light is rotated with a $\lambda/2$ plate to select either *p* or *s* polarization; only *p*-polarized 2PP spectra are reported unless a polarization dependence exists. Standard one-photon photoemission (1PP) with the fourth-harmonic (FH) of the fundamental pulse (6.1 eV) is employed to differentiate between the features in 2PP spectra that originate from the occupied or the unoccupied density of states (DOS). The FH is generated from the second harmonic with a 100 μm BBO crystal. Since phase matching in BBO can be achieved only to 407.5 nm, only the low-energy portion of the input spectrum can generate the FHG light. Consequently, the FHG power is too weak to measure (<1 mW), but sufficient to record 1PP spectra.

III. RESULTS AND DISCUSSION

A. Electronic structure of bare surfaces

Titanium dioxide is a wide band-gap semiconductor with a band gap of 3.05 eV for a stoichiometric rutile crystal.[25] The annealing process in vacuum and other methods of creating defects generate oxygen vacancies. The charge left over after desorption of surface bridging oxygen atoms remains associated with a pair of Ti^{3+} ions, whose coordination number drops to 5 and formal electron charge increases by 1.[4,26,27] Figure 1 shows the structure of the rutile $TiO_2(110)$

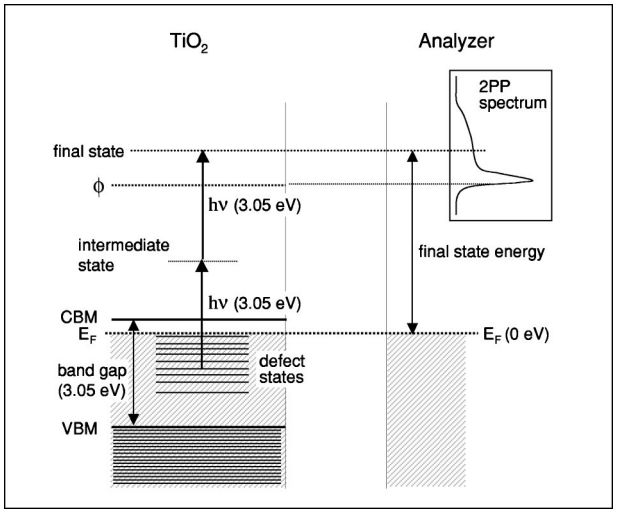

FIG. 2. Energy diagram of the defective TiO_2 crystal and 2PP measurement with the electron energy analyzer. E_F, ϕ, CBM, and VBM represent the Fermi level, the work function, the conduction band minimum, and the valence band maximum, respectively. In actual experiments the Fermi levels of the sample and the analyzer are offset by the 5 V bias voltage.

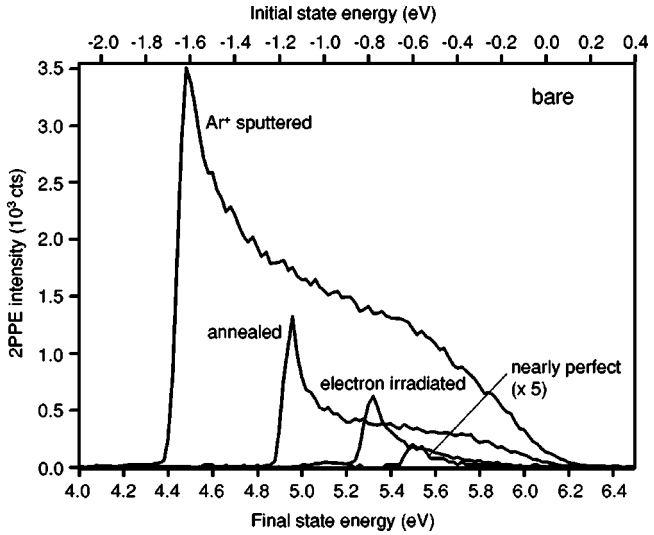

FIG. 3. 2PP spectra of nearly perfect, electron-irradiated, vacuum annealed, and Ar^+ sputtered surfaces at 100 K. The bottom and top horizontal axes give the final and initial state energy in two-photon excitation with respect to the Fermi level.

surface including a typical bridging oxygen vacancy. The DOS associated with these Ti^{3+} defects at the surface and related oxygen vacancies that diffuse into the bulk is centered at 0.8–1.0 eV below and extends up to the Fermi level.[28,29] Since the oxygen 2*p* state-derived valence bands start at 3 eV below the Fermi level on oxygen deficient surfaces, the introduction of these defects raises the Fermi level from midgap, where it would be for the perfect surface, to the bottom of the conduction band. The energy diagram for a defective TiO_2 crystal that shows the initial and intermediate levels contributing to 2PP spectra is shown in Fig. 2. Since the Fermi levels of both the TiO_2 crystal and the energy analyzer are always offset by the 5 V bias voltage, the photoelectron energy is always measured with respect to the Fermi level.

Figure 3 shows the 2PP spectra of bare $TiO_2(110)$ surfaces prepared by four different methods. The bottom and top horizontal axes represent final and initial state energies with respect to the Fermi level. The weakest spectrum measured at 100 K that rises from 5.5 eV is that of the nearly perfect surface. The second weakest spectrum starting at 5.3 eV is of the electron-irradiated surface prepared by exposure to a 0.48 mC/cm^2 dose of 500 eV electrons. The spectrum starting at 4.9 eV is that of an annealed surface prepared by heating the nearly perfect surface at 1000 K for 30 min in vacuum. Finally, the strongest and broadest spectrum is prepared by Ar^+ sputtering the nearly perfect surface for 20 min (1000 eV energy and 2 $\mu A/cm^2$ sample current). Note that the 2PP spectra in Fig. 3 are typical for these specific preparation methods; however, the intensities and work functions exhibit some variation between the same preparations due to factors that are beyond experimental control. In addition, the observed spectra are stable under laser excitation with either 3.05 or 6.1 eV excitation.

As shown in the energy diagram in Fig. 2, the high-energy edge in 2PP spectra around 6.1 eV above the Fermi level corresponds to two-photon photoemission of electrons from the Fermi level. Photoemission from the Fermi level is observed for all preparation methods, but the intensity at and near the Fermi level increases with the defect concentration. This is to be expected since the initial annealing procedure, which changes the sample color from transparent to blue and makes the sample conductive, introduces bulk defects that cannot be removed by subsequent surface preparation procedures. The low-energy edge is the minimum energy for excitation of an electron to a freely propagating state in vacuum, i.e., the work function. We confirmed this assignment by demonstrating that the low-energy edge coincides with the threshold energy for secondary electron emission when the sample is irradiated with 500 eV electrons. The lowest work function in Fig. 3 of 4.4 eV corresponds to photoemission from the initial states 1.7 eV below the Fermi level. Considering the large band gap and the pinning of the Fermi level just below the conduction band, photoemission can only occur from the defect states within the band gap; carriers excited from the top of the valence band to the bottom of the conduction band indicated in Fig. 2 have insufficient energy to be photoemitted by subsequent absorption of another 3.05 eV photon.

We define the half maximum of the lowest-energy edge of the 2PP spectra as the value of the work function for each surface. Based on this definition, work functions for the nearly perfect surfaces in our experiments range between 5.5–5.8 eV. Because the experimental accuracy is much better than the observed variation in the work function, the spread represents the variability in the surface preparation. Since the work function decreases with increasing defect density, the true work function is probably at the high limit of the observed range. These values are on the high end of previously reported values determined by UPS of 5.3 and 5.5 eV,[30,31] and probably indicate a lower defect density in our measurements. Also note that the electron irradiated surfaces characteristically often have a small subpeak below the

main work function threshold, which may indicate that the surface is inhomogeneous having regions of different work functions. The origin of this inhomogeneity is not understood, and this structure does not appear every time even though we follow the same preparation protocol.

Work function is one of the most fundamental properties of a solid surface, which rarely has been studied for metal oxides.[26] It is usually considered to be the sum of potentials required to overcome the bulk potential and to transport electrons through the surface bilayer.[32] The difference in work functions between different surface preparations can be explained by a simple model, which considers how the surface defects and adsorbates modify the surface potential. As in standard models for work functions of metals, the electron density extends beyond the image plane into the vacuum. The excess negative charge extending into vacuum is compensated by a net positive charge on the surface ions.[32] Since oxygen has strong electron affinity, which generates a negatively changed surface, the removal of oxygen reduces the negative charge, and therefore, reduces the work required to transport electrons into vacuum. Consequently, lower work function correlates with more surface oxygen vacancies.

A number of studies have shown that high-energy electrons and ions preferentially desorb oxygen ions and neutral atoms from TiO_2 surfaces generating vacancies.[33–36] Knotek and Feibelman[33,34] found that electrons with greater than 34 eV desorb surface oxygen through an interatomic Auger recombination process. XPS studies have shown that Ar^+ sputtering makes a rough surface with poorly defined stoichiometry that is depleted of oxygen.[37] Annealing at high temperature in vacuum also creates oxygen vacancies as evident from XPS, UPS, and STM experiments.[4,28,38] Therefore, we conclude from the 2PP spectra in Fig. 3 that the Ar^+ sputtered surface has the lowest oxygen concentration, followed by the annealed and the electron-irradiated surfaces. Further information on the near surface oxygen vacancies can be obtained from the oxygen molecule adsorption studies to be presented in the next section.

Compared with the changes in the work function, the difference in intensity distributions in 2PP spectra is not as easy to explain. Since the estimated electron escape depth at $\sim$6 eV is $\sim$3 nm,[32] the 2PP spectra are sensitive to both surface and bulk defects. The intensities in 2PP spectra depend on the joint occupied and unoccupied DOS, and to a lesser extent, the energy dependence of the transition moment coupling the initial, intermediate and final states.[14] The 2PP spectra also can have contributions from secondary electrons, which suffer energy and momentum changing collisions in the intermediate or final state prior to being emitted into vacuum. The secondary electron emission is sensitive to the surface quality and often forms a waning distribution at the work function edge, such as observed in most 2PP spectra reported here. In resonant UPS spectra, the Ti^{3+} defect DOS forms a peak symmetrically distributed about a binding energy of 0.8 eV;[28,29] however, in our spectra the defect induced signal decreases monotonically from the work function edge even for the sputtered surfaces that span the range from the Fermi level to 1.7 eV below the Fermi level. The reason why a distinct peak may not be observed can be attributed to several factors including the overlap of the Ti^{3+}

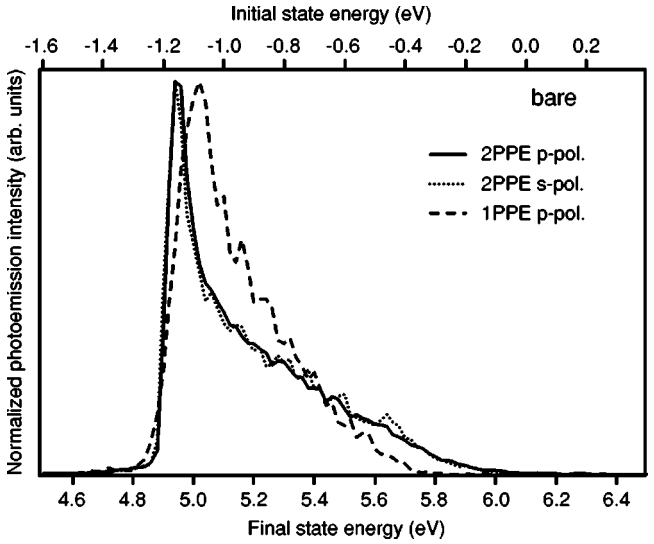

FIG. 4. Photoemission spectra of bare Ar^+ sputtered surface at 100 K measured with different modes of excitation. The solid and dotted lines, respectively, represent two-photon photoemission measured with *p* and *s* polarization with 3.05 eV light. The dashed line represents one-photon photoemission measured with *p*-polarized 6.1 eV light.

feature with secondary electrons, the convolution of the initial and intermediate state DOS in the 2PP spectra, the different final state resonance conditions, and the higher spectral resolution than in previous studies.

In order to further characterize the defect DOS, we excited photoemission with different polarizations and by one- and two-photon excitation to the same final state. Figure 4 compares normalized 2PP spectra of an Ar^+ sputtered surface excited with 3.05 eV *p*- and *s*-polarized light and 1PP excited with the 6.1 eV *p*-polarized light. The 2PP spectra are independent of the polarization and differ slightly from the 1PP spectrum. The enhancement of 2PP spectra at the Fermi edge with respect to the 1PP spectrum may be due to a contribution to the joint DOS from the e_g symmetry Ti^{4+} intermediate states starting at $\sim$2 eV above the conduction band.[39] The difference in the work function edges between 1PP and 2PP spectra is probably related to a larger laser spot size used in 1PP measurements, which results in the averaging over a larger area of a nonuniform surface (the actual beam size and location could not be determined due to its low power level). It is also interesting to note that the *s*- and *p*-polarized spectral distributions are identical: this is to be expected only for a disordered surface, since the two polarizations couple states of different symmetry with respect to the surface normal.[18]

We conclude that the photoemission spectra in Figs. 3 and 4 are mainly due to the initial states that exist in the fundamental band gap of TiO_2 on account of defects. These states can be generated with different distributions by various preparation techniques. The low-energy edge of 2PP spectra gives an accurate value of the work function averaged over the irradiated spot on the surface. The 2PP spectra are quite sensitive to the work function changes, because the photoemission system is optimized for detection of much lower-

energy electrons than in standard UPS experiments. We exploit this ability to measure work functions to study the effect of molecular adsorption on the electronic structure of TiO_2 surfaces.

B. Oxygen adsorption

Following O_2 adsorption, we investigate the work function change produced with different surface preparations. Molecular oxygen is adsorbed on TiO_2 surfaces at 100 K and spectra are taken after specific doses measured in Langmuir ($1\ L = 10^{-6}$ Torr s). Before the measurements, we made sure that the spectra are stable with 3.05 eV laser irradiation, even though the photodesorption of weakly bound O_2 molecules with photon energies above 3.1 eV has been observed with photodesorption methods[9] and surface second harmonic generation methods.[40] Exposing the nearly perfect surfaces to 5 L of O_2 does not change the 2PP spectra (not shown). This result is consistent with other observations and theoretical predictions that O_2 does not adsorb on a perfect surface even at 100 K.[7,9,27]

By contrast, the O_2 adsorption on electron-irradiated (500 eV energy; 0.48 mC/cm^2 dose) surface shown in Fig. 5 produces dramatic changes in the 2PP spectra. The thick solid line in Fig. 5(a) is for the bare electron-irradiated surface, while the much less intense spectra are of the oxygen-exposed surfaces. We also show for comparison the initial nearly perfect surface. Since the 2PP intensity is substantially reduced by the O_2 exposure, Fig. 5(b) shows expanded spectra in the indicated region of Fig. 5(a). Low photoelectron count rates are responsible for the jagged appearance of the expanded spectra. The thin solid lines in Fig. 5(b) represent photoemission after exposing the surface to 0.06 and 0.30 L of O_2, while the dashed line represents the nearly perfect surface before the electron irradiation. Further O_2 dosing does not change the 2PP spectra. *Remarkably, exposure to only a fraction of a monolayer of O_2 restores the nearly perfect surface spectrum at 100 K*. After the O_2 exposure, the surface is further heated up to 450 K for a minute and cooled back to 100 K. The 2PP spectrum after this heating procedure is shown by the dotted line in Fig. 5(b). There is almost no change in the 2PP spectra after the heating procedure, indicating that the surface is restored to the nearly perfect condition at 100 K.

Our observation of defect healing at 100 K contrasts those of Henderson[7] and Lu[9] *et al.* who report that for *vacuum annealed* surfaces healing of oxygen vacancies requires heating of the surface to temperature in the range of 150 to 400 K. We will show below that these activated healing processes may involve subsurface oxygen defects that exist on annealed surfaces, but not on electron irradiated surfaces. Our observation of efficient healing at 100 K after submonolayer exposure suggests that O_2 is adsorbed with a high probability in a weakly bound state with high surface mobility. Henderson *et al.* give 0.5–0.6 as the initial sticking probability for the annealed surface at 120 K.[7] The efficient healing implies that mobile, weakly bound O_2 is irreversibly trapped either as a peroxo O_2^{2-} species, or that it dissociates into O^{2-} at the bridge site vacancy. Density functional theory

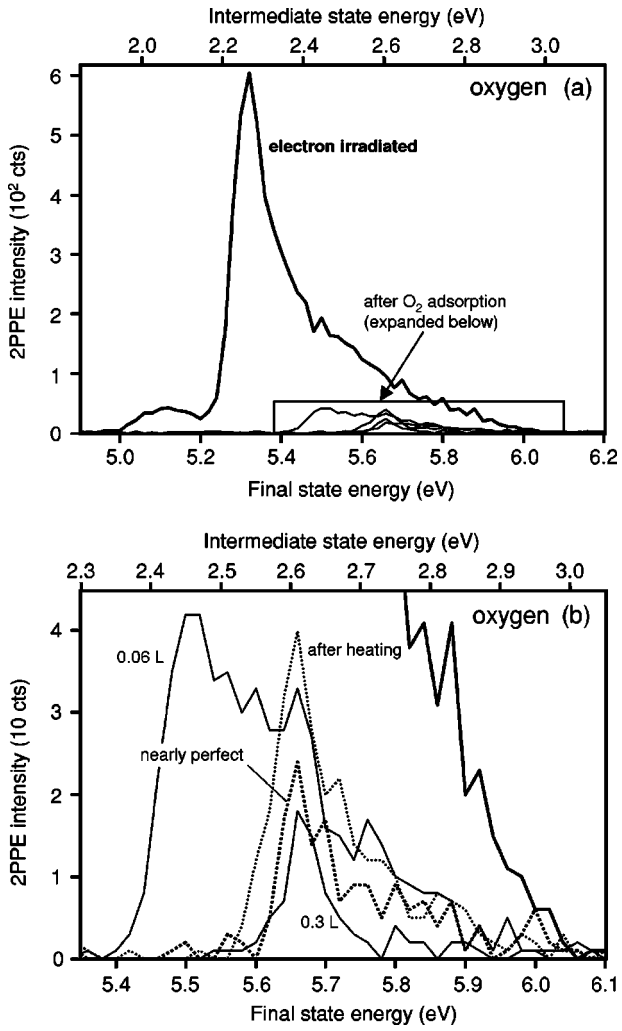

FIG. 5. (a) 2PP spectra of electron-irradiated surface at 100 K before and after exposure to oxygen molecules. The bottom and top horizontal axes represent the final and intermediate state energy with respect to the Fermi level. The thick solid line is the bare surface after electron irradiation with a 0.48 mC/cm^2 dose of 500 eV electrons. (b) Expanded spectra in the indicated region from (a). The dashed line gives the nearly perfect surface before electron irradiation. Thin solid lines give the electron-irradiated surface after exposure to 0.06 and 0.3 L of O_2. The dotted line represents the spectrum after heating the oxygen-exposed surface to 450 K and subsequent cooling to 100 K.

(DFT) calculations show that the above molecular and atomic species have similar adsorption energies of 2.5–3.0 eV, and that the barrier to interconversion is on the order of 1 eV; however, the dissociative adsorption is entropically favored.[27,41] Henderson *et al.* proposed that the dissociation of O_2 at defect sites generates a strongly bound O^{2-} that heals the Ti^{3+} defect and a weakly bound O atom that remains in the channel between the bridging oxygen rows.[42] A similar structure has been proposed by Schaub to explain the high mobility of defects observed by STM.[8] We find no spectroscopic evidence for O_2^{2-} or for this weakly bound O atom perhaps because they do not contribute distinct spectroscopic features to our spectra. We also note that the healing of defects on the electron irradiated surface oc-

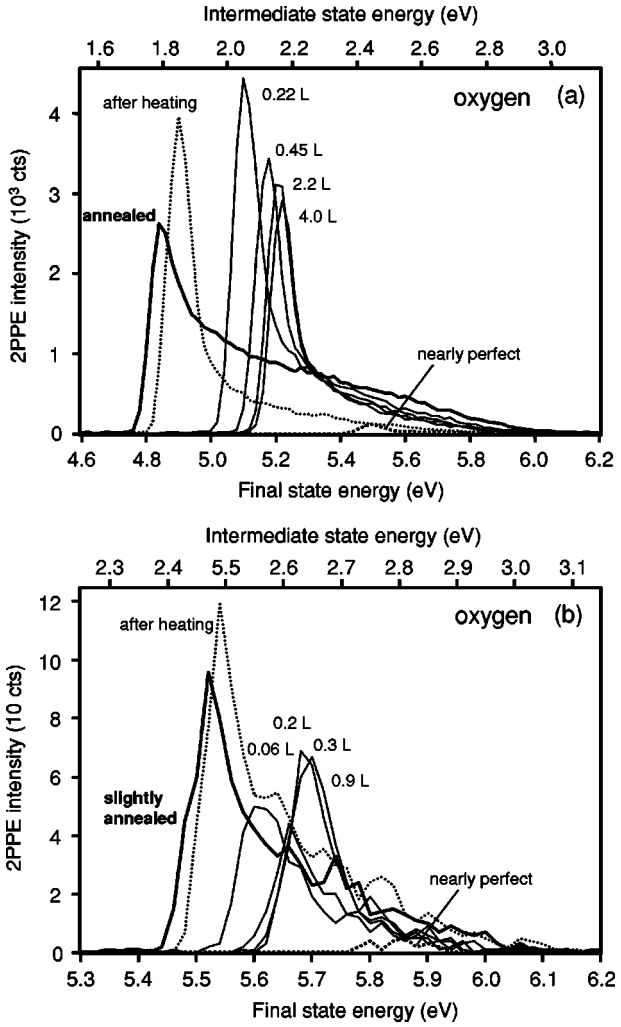

FIG. 6. 2PP spectra of vacuum annealed surfaces before and after exposure to oxygen. a) The annealed surface prepared by heating to 1000 K for 30 min in vacuum. (b) Less strongly reduced surface prepared by heating to 900 K for 10 min. In both figures, dashed lines represent the clean surface taken at 100 K immediately after the preparation. The thin solid lines represent spectra of oxygen-exposed surface for several dosages. The dotted lines represent the oxygen-exposed surface spectra after heating to 450 K and subsequent cooling to 100 K.

curs at 100 K without a significant activation energy barrier, whereas according to Rasmussen's calculation the barrier to O_2 dissociation is 1 eV.[27]

The same O_2 adsorption/heating procedure is repeated for the vacuum annealed surface (1000 K for 30 min), which is cooled to 100 K before the measurements. The 2PP spectra (thick solid line) in Fig. 6(a) show that this treatment reduces the work function by 0.7 eV and significantly increases the intensity compared with the nearly perfect surface (dashed line). The annealed surface is exposed to a range of O_2 doses (0.1 to 4.0 L) and 2PP spectra shown by thin solid lines are taken after each exposure. By contrast with the electron-irradiated surface, the work function of oxygen-exposed surface increases more gradually as the dosage is increased, and even after exposure to 4.0 L of O_2 the spectrum does not return to that of the nearly perfect surface. After the O_2 exposure, the work function saturates at 5.2 eV, which is substantially below that of the nearly perfect surface. The 2PP intensities also change in a complex manner during the exposure, and do not decrease like for the electron-irradiated surface. The behavior of vacuum annealed surface is also substantially different after the heating procedure (dotted line): the work function reverts to that of the original annealed surface, although the intensity at high energies is decreased by this procedure.

Since there is a possibility that the heavy annealing procedure creates a drastically different surface compared to the electron-irradiated surface, we also prepared a "slightly annealed" surface by heating the sample in vacuum at 900 K for 10 min. Compared with strong annealing this procedure generates more modest changes in the 2PP spectra. Although the work function change (−0.4 eV) is comparable to the electron-irradiated surface, the behavior upon O_2 dosing and heating shown in Fig. 6(b) is entirely consistent with the trends observed for the heavily annealed surface. The only difference between heavily and lightly annealed surfaces is the O_2 dose at which the changes saturate, which decreases to ~1 L. The results in Figs. 5 and 6 lead us to conclude that the electron irradiation and vacuum annealing produce defects with substantially different properties as evidenced by 2PP spectra. The response of electron irradiated and vacuum annealed surfaces to O_2 differs significantly.

The different sensitivity of the electron-irradiated and annealed surfaces to oxygen exposure probably reflects different distributions of defects produced by each preparation method. It is difficult to distinguish the surface and bulk defects of TiO_2 by 2PP because their spectra seem to overlap, and furthermore, photoemission probes the electronic structure over a 3 nm escape depth for electrons corresponding to about 20 layers.[4] Even the work function, which is mainly sensitive to the surface bilayer, can be modified by near-surface defects. Thermal annealing of the surface will produce a distribution of defects that is determined by thermodynamic and kinetic considerations, namely, their relative stability and the rates of defect generation at the surface and diffusion into the bulk. With electron irradiation, the defects are generated mainly at the surface, but at 100 K their diffusion into the bulk is suppressed. Thus, on the bare electron-irradiated surface, the work function and intensity distribution of 2PP spectra are determined by the surface defects, which are mainly bridging oxygen vacancies. Molecular oxygen effectively heals the surface defects at 100 K, and therefore, the 2PP spectra are restored to that of a nearly perfect surface. By contrast, for the bare annealed surface the 2PP spectrum is probably dominated by subsurface defects, because the integration of the bulk defect signal over the 20 layer escape depth can easily overwhelm the surface contribution. The sharp increase of the 2PP intensity at the work function edge is probably due to the secondary electrons, which are generated efficiently at rough or disordered surfaces. Oxygen adsorption can heal the surface defects and therefore produce a substantial increase in the work function. However, the secondary electron intensity does not decrease indicating that the near-surface region is still disordered. The resulting surface is different from the nearly perfect surface because the work function change is not complete. Accord-

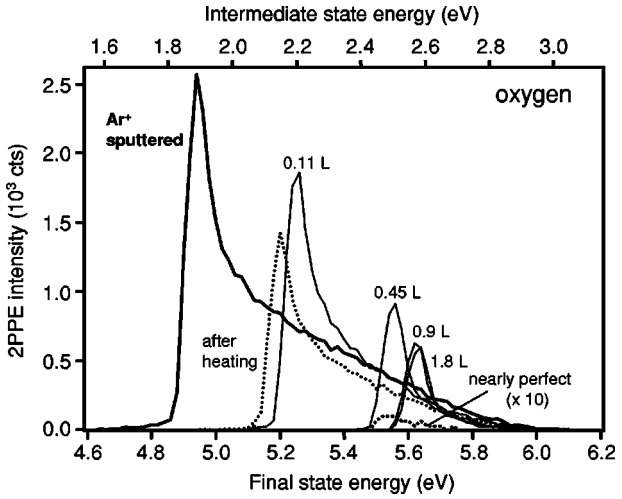

FIG. 7. 2PP spectra of Ar^+ sputtered surfaces before and after exposure to oxygen. The dashed line is the spectrum of the nearly perfect surface expanded ten times. The thick solid line is the bare Ar^+ sputtered surface prepared by exposing the surface to 1000 eV Ar^+ beam for 20 min. Thin solid lines represent the spectra of oxygen-exposed surface for several dosages. The dotted line represents the oxygen-exposed surface spectra after heating to 450 K and subsequent cooling to 100 K.

ing to Lu[9] and Henderson *et al.*[7] this surface supports molecularly adsorbed species that are photochemically labile and whose dissociation to atomic species is activated in a temperature range of 150–400 K. Since O_2 does not adsorb on the nearly perfect surface even at 100 K, we propose that the O_2 adsorption and activated defect healing on vacuum annealed surfaces involves subsurface defects as well as surface defects. The activated dissociation may arise from the diffusion of existing subsurface defects to the surface where they can be healed with the preadsorbed O_2 molecules. In STM images of annealed $TiO_2(110)$ surfaces, two types of oxygen vacancies with densities of 7 and 1–2 % have been assigned, respectively, to the surface bridging oxygen vacancy, because it is selectively healed by O_2 adsorption, and to subsurface oxygen vacancies.[43] Our results suggest that it should also be possible to selectively generate and identify surface vacancies with STM by the comparison of electron irradiated and annealed surfaces. Moreover, theoretical investigation of the interaction of adsorbates with subsurface defects may provide further understanding of surface chemistry of TiO_2.

Finally, Fig. 7 presents the spectral changes following the interaction of O_2 with Ar^+ sputtered surface (10 min, 1000 V) using the same procedures as above. Exposing the bare Ar^+ sputtered surface to O_2 increases the work function to 0.1 eV *above* that of the nearly perfect surface. However, the 2PP spectra after O_2 exposure have much higher intensity than the nearly perfect surface indicating that some defects cannot be healed at 100 K. By heating, the work function is reduced as in the case of the annealed surface, but the shift does not extend as low as the original sputtered surface.

Argon ions, similar to electrons, cause nonthermal damage to the surface. However, Ar^+ can transfer much larger momentum to the surface and therefore induce much more damage, including subsurface defects. XPS measurements show evidence for defects with the valence of titanium Ti^{n+} ranging from 0–3.[44] These vacancies cause strong intensity and very low work function in the 2PP spectra. When exposed to oxygen, a significant fraction of vacancies is healed because they exist mainly at the outermost layer. The reason why the work function exceeds that of the nearly perfect surface is not understood, but it is certain that the exposure of the highly nonstoichiometric surface to O_2 at 100 K cannot return the surface to the perfect stoichiometry. It is possible that the concentration of oxygen on the sputtered surfaces after saturation exposure is even larger than for the stoichiometric surface, leading to a higher work function. Some of the oxygen species are labile, so the heating reduces the oxygen concentration as indicated by the reduced work function.

The results on interaction of oxygen molecules with nearly perfect and damaged TiO_2 surfaces demonstrate that the high sensitivity of 2PP to the work function and the concentration of near surface defects. The 3.05 eV excitation can only induce two-photon photoemission from the defect states hence it provides considerably higher sensitivity to defects as compared with more standard surface science techniques.

C. Water adsorption

We prepared the four different surfaces and exposed them to water vapor in the same manner as for the oxygen-adsorption experiments. Figures 8 and 9 show the results for the nearly perfect, electron-irradiated, annealed, and Ar^+ sputtered surfaces. In all cases, water causes a work function shift in the opposite direction to oxygen, indicating that it acts as an electron donor rather than an acceptor even for highly reduced surfaces. As the dosage is increased, the work function decreases and the 2PP intensity increases. The work function change saturates at a dose of ~5 L. As shown in some of the data, a small subpeak corresponding to a surface with a lower work function often appears for water adsorption, but its intensity and location are not reproducible. We assume that as for the electron-irradiated clean surface, it originates from domains with a lower work function. Since its origin is unknown and its intensity and work function relative to the main spectrum are not reproducible between sample preparations, we focus exclusively on the main spectrum.

In order to extract more quantitative information on the interaction between water and TiO_2 surfaces, in Fig. 10(a) we plot the work function change of the main threshold for all surfaces as a function of dosage. As seen in Fig. 10(a), the work function change in the range of −0.8 to −1.2 eV saturates after exposure to ~5 L of water, and by contrast to oxygen, adsorption appears to be weakly dependent on the defect concentration. According to Henderson, 1.8 L exposure of water on TiO_2 corresponds to one monolayer.[10] The saturation behavior indicates that only the initial growth forms a film with ordered dipole moments and in subsequent layers, the dipole moment is random or parallel to the sur-

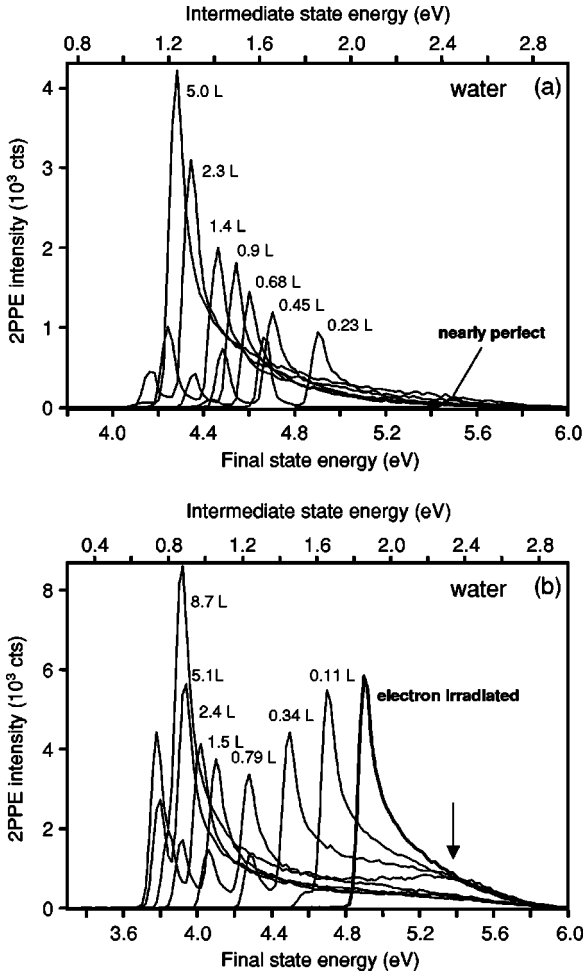

FIG. 8. 2PP spectra of bare and water-exposed surfaces at 100 K: (a) nearly perfect surface and (b) electron-irradiated surface after a 1.6 mC/cm^2 dose of 500 eV electrons. The thick solid lines represent the bare surfaces and thin solid lines represent water-exposed surfaces for different dosages.

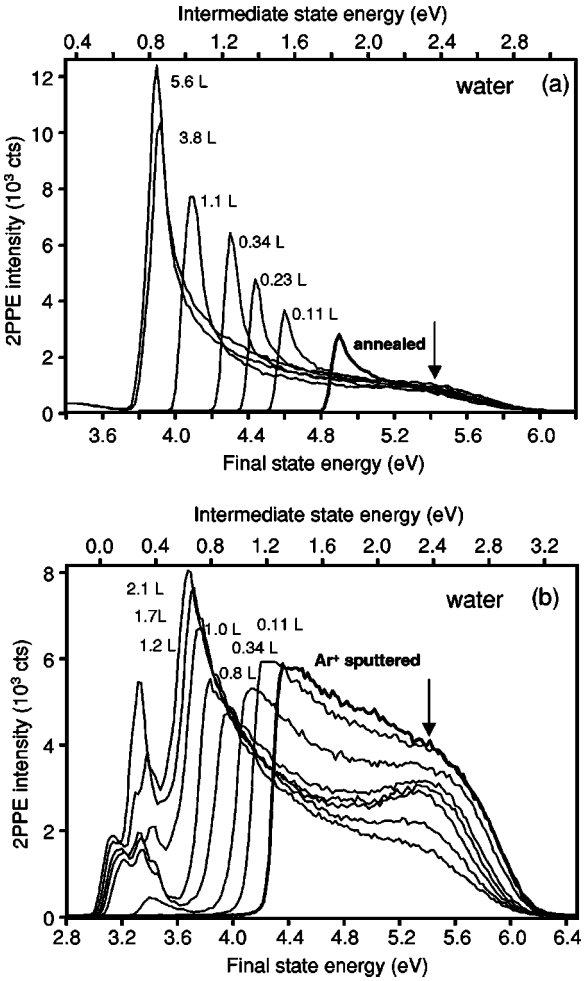

FIG. 9. 2PP spectra of bare and water- exposed surfaces at 100 K: (a) annealed surface prepared by heating at 1000 K for 30 min in vacuum and (b) Ar^+ sputtered surface prepared by exposure to a 1500 eV Ar^+ beam for 15 min. The thick solid lines represent the bare surfaces and thin solid lines represent water-exposed surfaces for different dosages.

face. This magnitude of work function change is comparable to the only other measurement of work function for $H_2O/TiO_2(110)$ by Hugenschmidt *et al.*[45] The variation in the high-coverage work function does not appear to be strongly influenced to the initial surface defect concentration, but rather it probably depends on the adsorption and ordering of water molecules on the surface in the channel between the bridging oxygen rows. The limit of the work function probably depends on such factors as the rate of adsorption and the concentration of nucleation centers for island formation that is difficult to control experimentally.

Henderson proposed a structure for water multilayer adsorption on $TiO_2(110)$ surface based on TPD and HREELS measurements.[10] According to this model, the first layer water molecules adsorbs in channels between the bridging oxygen atoms with adsorbate oxygen atoms interacting with terminal Ti^{4+} sites and hydrogen atoms pointing into vacuum. This assignment was proposed to explain the absence of hydrogen bonding between water molecules in HREELS spectra. Henderson concluded that water molecules make separate networks between the first and second layers based on the observation that strong hydrogen bonding within the second layer occurs with retention of the nonhydrogen bonded OH stretch of the first layer molecules. Our results are consistent with his conclusion in that it appears that only the first layer of water adsorbed at the terminal Ti^{4+} sites contributes to the work function change.

We analyze the change in the work function of TiO_2 upon adsorption of H_2O based on the Helmholtz model, where the molecules are treated as a surface dipole layer:[32,46]

$$\Delta\phi = \frac{Ne\mu_{\text{eff}}}{\epsilon_0}. \tag{1}$$

According to this model, the work function change $\Delta\phi$ is proportional to density of molecules N and their effective dipole moment μ_{eff} (e and ϵ_0 are electron charge and dielectric constant of free space, respectively).

We assume that molecules adsorb at every terminal Ti^{4+} site to estimate their density on the surface. To simulate the data in Fig. 10(b), we derive a simple equation to describe

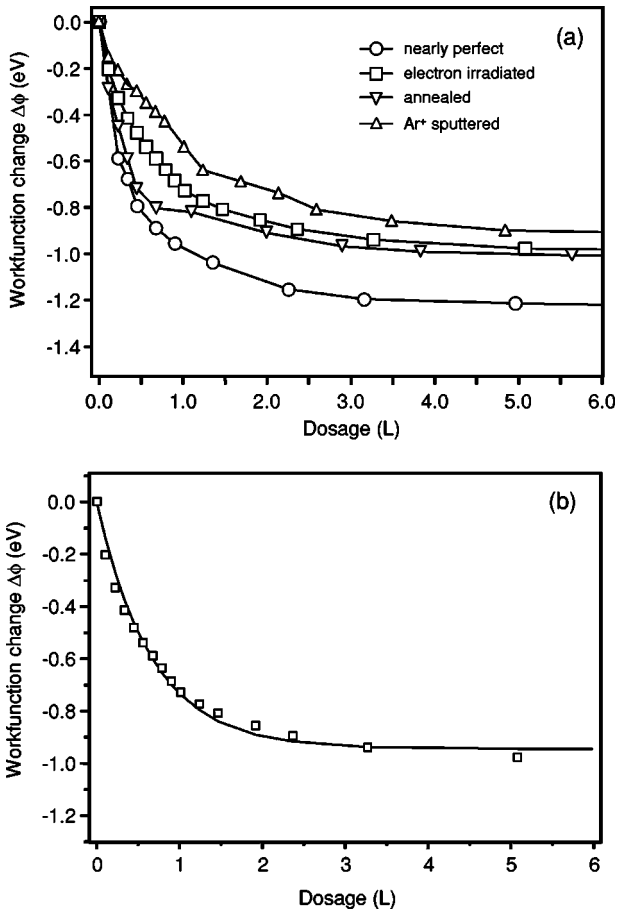

FIG. 10. (a) The work function change as a function of water dosage for nearly perfect, electron-irradiated, vacuum-annealed, and Ar^+ sputtered surfaces. Lines connect individual data points to guide the eye. (b) Experimental data (squares) and simulation curve (solid line) of work function change as a function of dosage for the electron-irradiated surface. The simulation curve is obtained by a least-squares fit of the experimental data to Eq. (4), where the best fit parameters are $\mu_{\text{eff}}=0.48\pm0.01$ D and $k=1.49\pm0.07$ L^{-1}.

the work function change as a function of H_2O dosage. The expression in Eq. (1) models the bilayer as a parallel-plate capacitor. To model a monolayer of molecules we replace the dielectric constant of vacuum with ϵ, where $\epsilon=\epsilon_0(1+\chi)$ represents the dielectric function of the water film. MacDonald and Barlow derived a relationship for the susceptibility χ of the monolayer in terms of the molecular polarizability α[47]

$$4\pi\chi=\alpha\Lambda N^{3/2}. \tag{2}$$

Λ is the molecular structure parameter with approximate value of 9 ($\Lambda=8.894$ for a hexagonal array and $\Lambda=9.034$ for a square array). From Eqs. (1) and (2), we derive

$$\Delta\phi(x)=\frac{Ne\mu_{\text{eff}}}{\epsilon_0\left[1+\frac{\Lambda}{4\pi}\alpha N^{3/2}\right]}. \tag{3}$$

To fit the data we also need to know the coverage of water. We assume the Langmuir adsorption equation $\theta=1-\exp(-kx)$, where θ is the coverage, x is the dosage, and the constant k includes all effects concerning the adsorption probability, for example, the sticking probability and uncertainty in the pressure measurement. We also use the relationship $N=\theta N_0$, where N_0 is the density of molecules per unit area at full coverage. Combining the above equations, we obtain the change in the work function as function of exposure,

$$\Delta\phi(x)=\frac{e\mu_{\text{eff}}N_0[1-\exp(-kx)]}{\epsilon_0\left(1+\frac{\Lambda}{4\pi}\alpha\{N_0[1-\exp(-kx)]\}^{\frac{3}{2}}\right)}. \tag{4}$$

We use $N_0=0.52\times10^{15}$ cm^{-2} assuming that the density of water molecules is equal to that of terminal Ti^{4+} ions.[10] Equation (4) has three variable parameters: μ_{eff}, α, and k, which we can be deduced by a least-squares fit to the data. However, it turns out that because $1/(1+c\alpha)$, where c is constant, and $1-\exp(x)$ are very similar functions, α and k are strongly correlated making it impossible to derive the value of each independently. In fact, $c\alpha$ is estimated to be the order of 10^{-9} from the polarizability of the free water molecule of 1.45×10^{-24} cm^3. This value is much smaller than 1 in the denominator of the equation, thus we make the usual approximation of setting $\alpha=0$. If the relation between the work function and coverage is linear, this assumption is justified and μ includes all effects of α.[48]

The solid curve in Fig. 10(b) represents a sample least-squares fit using Eq. (4) for the electron-irradiated surface. The curve reproduces well our experimental data. The derived dipole moment μ_{eff} is 0.48 ± 0.01 D and $k=1.49\pm0.07$ L^{-1}. The dipole moments for other surfaces range between 0.45–0.6 D. Our results are consistent with a previous measurement of $\mu_{\text{eff}}=0.5$ D for water on a nearly perfect $TiO_2(110)$ surface by XPS.[45] The dipole moment of water adsorbed on Ir(110),[49] Cu(110),[50] and Cu(100) (Ref. 50) surfaces is reported to be 0.4, 0.87, and 0.5 D, respectively, for $\alpha=0$. The effective dipole moment on metal and oxide surfaces is considerably smaller than for free water molecules in the gas phase where $\mu=1.854$ D.[51] The similarities between the effective dipole moments on oxide and metal surfaces can in part be attributed to dipole-dipole depolarization,[52] which is common to all ordered films, but it also suggests that substrate water interactions,[53] are also similar. Finally, we note that the agreement with the Langmuir adsorption kinetics for at least the first monolayer implies that well-ordered $TiO_2(110)$ surfaces under UHV are hydrophilic.

In contrast to the oxygen adsorption, the 2PP spectra of water-adsorbed surfaces do not depend significantly on the surface preparation and their work function changes fit well to the same theoretical model. The result indicates that water molecules adsorb on the terminal Ti^{4+} ion, which appears to be the main surface feature regardless of the surface preparation, and only the first layer contributes to work function change. There is now strong experimental and theoretical evidence that water dissociates to form pairs of surface hydroxyl ligands;[4,10,28,45,54,55] however, the dissociation at minority defect sites does not seem to have substantial effect on the work function change.

In addition to the work function change, the adsorption of water leads to another notable spectral feature that exclu-

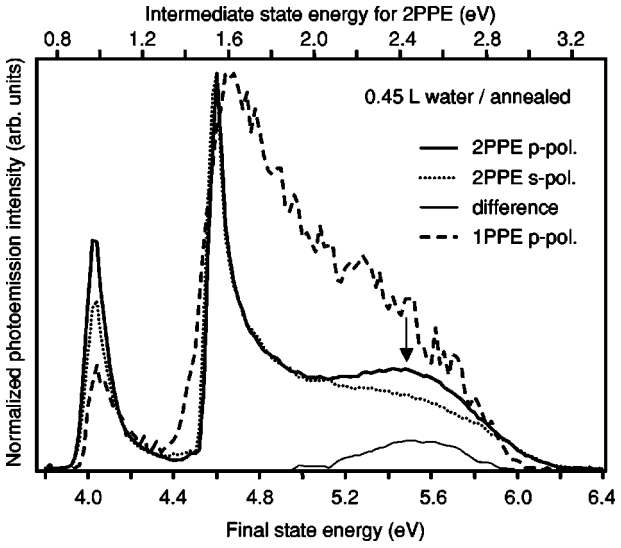

FIG. 11. Photoemission spectra of water-exposed annealed surface with different modes of excitation. The thick solid and dotted lines represent, respectively, 2PP spectra measured with *p* and *s*-polarized 3.05 eV excitation. The dashed line gives the 1PP spectrum measured with *p*-polarized 6.1 eV light. The arrow indicates the water-induced unoccupied state at 2.45 eV that is only observed for less than one monolayer water coverage in *p*-polarized 2PP spectra. In order to show the water-induced peak clearly, the difference spectrum between the normalized spectra measured with *p* and *s* polarization is also shown by the thin solid line.

sively appears for surfaces with introduced defects. A broad, low intensity band that is indicated by arrows in Figs. 8 and 9 appears at the final state energy of ~5.5 eV. This peak reaches the maximum intensity after exposure to 1 L of H_2O and greatly decreases in intensity at higher dosages. This feature is never observed on nearly perfect surfaces. The comparison of 2PP spectra recorded with *s* and *p* polarization in Fig. 11 shows that the water-induced peak can only be excited with *p* polarization. In order to show the water-induced peak clearly, the difference spectrum between the *p*- and *s*-polarized spectra that have been normalized in the 4.6–4.9 eV region is shown for the 5.5 eV region in Fig. 11. Such polarization dependent differences do not occur when O_2 is adsorbed on TiO_2 surfaces. Figure 11 also shows 1PP spectrum of the same surface, which does not show the water-induced band. The fact that the band appears exclusively in the *p*-polarized 2PP spectra indicates that it is due to an unoccupied intermediate state resonance that has a transition moment normal to the surface. These observations clearly point to assignment to an unoccupied resonance at 2.45 eV that is induced by water adsorption, and probably involves substrate-adsorbate or intra-adsorbate excitation. Details of this direct observation of an unoccupied electronic state by electronic spectroscopy on an oxide surface will be reported in a future publication.[56]

IV. CONCLUSION

We have measured 2PP spectra of various $TiO_2(110)$ surfaces with femtosecond laser excitation at 3.05 eV. The 2PP signal is exclusively from defect states that exist in the band gap of nonstoichiometric $TiO_2(110)$ surfaces. This allowed us to examine the relative defect densities and work functions of nearly perfect, electron and ion damaged, and vacuum annealed surfaces. Since the different surface preparation methods mostly affect the concentration and distribution of surface and bulk oxygen vacancies, the work function change is a sensitive probe of removal of the electronegative O^{2-} ions.

Since the oxygen vacancy defects play an important role in the surface chemistry of TiO_2 surfaces, we examined the interaction of differently prepared surfaces with atmospheric gases O_2 and H_2O. We find based on work function changes that O_2 efficiently heals most of the surface defects on electron irradiated TiO_2 surface even with submonolayer exposures at 100 K. By contrast, the defects are not completely healed for Ar^+ sputtered and high-temperature annealed surfaces presumably because these contain defects other than surface bridging oxygen vacancies. These unidentified defects could be subsurface vacancies or more highly reduced surface species than exist on electron irradiated surfaces, which bind oxygen probably in the molecular form that can be desorbed by heating the surface to 450 K.

Finally, we measured 2PP spectra of water-adsorbed surfaces at various dosages. The work function change was explained by a simple electrostatic model by contrast to the oxygen adsorption. The work function change can be understood by water molecules adsorbing at the terminal Ti^{4+} sites, which predominate on all surfaces independent of specific preparation. The work function change can be explained by adsorption of a monolayer of water according to Langmuir adsorption kinetics where the effective dipole moment contributed by water is 0.5 D. This value is comparable to 0.4–0.9 D observed for water on metal surfaces. We also found an unoccupied band, which appears at 2.45 eV above the Fermi level for submonolayer coverage of water; its assignment is currently under investigation.

ACKNOWLEDGMENTS

This work was supported by the DOD Multidisciplinary University Research Initiative (MURI) program administered by the Army Research Office under Grant No. DAAD19-01-1-0619. The apparatus for time-resolved two-photon photoemission has been developed with partial support from NSF Grant No. DMR-0116034. The authors acknowledge the critical reading of this manuscript, invaluable discussions, and support from Professor J. T. Yates, Jr. and members of his group.

*Electronic address: petek@pitt.edu

[1] A. Fujishima and K. Honda, Nature (London) **238**, 27 (1972).
[2] M. Grätzel, Comments Inorg. Chem. **12**, 93 (1991).
[3] A. L. Linsebigler, G. Lu, and J. T. Yates, Jr., Chem. Rev. (Washington, D.C.) **95**, 735 (1995).
[4] U. Diebold, Surf. Sci. Rep. **48**, 53 (2003).
[5] K. Sunada, Y. Kikuchi, K. Hashimoto, and A. Fujishima, Environ. Sci. Technol. **32**, 726 (1998).
[6] A. Nakajima, K. Hashimoto, T. Watanabe, K. Takagi, G. Yamauchi, and A. Fujishima, Langmuir **16**, 7044 (2000).
[7] M. A. Henderson, W. S. Epling, C. L. Perkins, C. H. F. Peden, and U. Diebold, J. Phys. Chem. B **103**, 5328 (1999).
[8] R. Schaub, E. Wahlström, A. Ronnau, E. Lægsgaard, I. Stensgaard, and F. Besenbacher, Science **299**, 377 (2003).
[9] G. Lu, A. L. Linsebigler, and J. T. Yates, Jr., J. Chem. Phys. **102**, 4657 (1995).
[10] M. A. Henderson, Surf. Sci. **355**, 151 (1996).
[11] R. Wang, K. Hashimoto, A. Fujishima, M. Chikuni, E. Kojima, A. Kitamura, M. Shimohigoshi, and T. Watanabe, Nature (London) **388**, 431 (1997).
[12] M. Miyauchi, N. Kieda, S. Hishita, T. Mitsuhashi, A. Nakajima, T. Watanabe, and K. Hashimoto, Surf. Sci. **511**, 401 (2002).
[13] *Solid-state Photoemission and Related Methods*, edited by W. Schattke and M. A. V. Hove (Wiley, Weinheim, 2003).
[14] H. Petek and S. Ogawa, Prog. Surf. Sci. **56**, 239 (1997).
[15] M. Weinelt, J. Phys.: Condens. Matter **14**, R1099 (2002).
[16] U. Höfer, I. L. Shumay, C. Reuss, U. Thomann, W. Wallauer, and T. Fauster, Science **277**, 1480 (1997).
[17] I. L. Shumay, U. Höfer, C. Reuss, U. Thomann, W. Wallauer, and T. Fauster, Phys. Rev. B **58**, 13 974 (1998).
[18] S. Ogawa, H. Nagano, and H. Petek, Phys. Rev. B **55**, 10 869 (1997).
[19] E. Knösel, A. Hotzel, and M. Wolf, Phys. Rev. B **57**, 12 812 (1998).
[20] H. Petek, M. J. Weida, H. Nagano, and S. Ogawa, Science **288**, 1402 (2000).
[21] H. Petek, H. Nagano, M. J. Weida, and S. Ogawa, J. Phys. Chem. B **105**, 6767 (2001).
[22] L. Bartels, G. Meyer, K.-H. Rieder, D. Velic, E. Knösel, A. Hotzel, M. Wolf, and G. Ertl, Phys. Rev. Lett. **80**, 2004 (1998).
[23] C. Gahl, K. Ishioka, Q. Zhong, A. Hotzel, and M. Wolf, Faraday Discuss. **117**, 191 (2000).
[24] X.-Y. Zhu, Annu. Rev. Phys. Chem. **53**, 221 (2002).
[25] H. Tang, F. Lévy, H. Berger, and P. E. Schmid, Phys. Rev. B **52**, 7771 (1995).
[26] V. E. Henrich and P. A. Cox, *The Surface Science of Metal Oxides* (Cambridge University Press, Cambridge, 1994).
[27] M. D. Rasmussen, L. M. Molina, and B. Hammer, J. Chem. Phys. **120**, 988 (2004).
[28] R. L. Kurtz, R. Stockbauer, T. E. Madey, E. Román, and J. L. de Segovia, Surf. Sci. **218**, 178 (1989).
[29] K. A. See and R. A. Bartynski, J. Vac. Sci. Technol. A **10**, 2591 (1992).
[30] Y. W. Chung, W. J. Lo, and G. A. Somorjai, Surf. Sci. **64**, 588 (1977).
[31] H. Onishi, T. Aruga, C. Egawa, and Y. Iwasawa, Surf. Sci. **193**, 33 (1988).
[32] G. A. Somorjai, *Introduction to Surface Chemistry and Catalysis* (Wiley, New York, 1994).
[33] M. L. Knotek and P. J. Feibelman, Phys. Rev. Lett. **40**, 964 (1978).
[34] P. J. Feibelman and M. L. Knotek, Phys. Rev. B **18**, 6531 (1978).
[35] S. Eriksen and R. G. Egdell, Surf. Sci. **180**, 263 (1987).
[36] L.-Q. Wang, D. R. Baer, and M. H. Engelhard, Surf. Sci. **320**, 295 (1994).
[37] W. Göpel, J. A. Andersion, D. Frankel, M. Jaehnig, K. Phillips, J. A. Schaefer, and G. Rocker, Surf. Sci. **139**, 333 (1984).
[38] M. Li, W. Hebenstreit, U. Diebold, A. M. Tyryshkin, M. K. Bowman, G. G. Dunham, and M. A. Henderson, J. Phys. Chem. B **104**, 4944 (2000).
[39] S. Munnix and M. Schmeits, Phys. Rev. B **30**, 2202 (1984).
[40] A. N. Shultz, W. Jang, W. M. Hetherington III, D. R. Baer, L.-Q. Wang, and M. H. Engelhard, Surf. Sci. **339**, 114 (1995).
[41] X. Wu, A. Selloni, M. Lazzeri, and S. K. Nayak, Phys. Rev. B **68**, 241402 (2003).
[42] W. S. Epling, C. H. F. Peden, M. A. Henderson, and U. Diebold, Surf. Sci. **412/413**, 333 (1998).
[43] U. Diebold, J. Lehman, T. Mahmoud, M. Kuhn, G. Leonardelli, W. Hebenstreit, and P. Varga, Surf. Sci. **411**, 137 (1998).
[44] J. T. Mayer, U. Diebold, T. E. Madey, and E. Garfunkel, J. Electron Spectrosc. Relat. Phenom. **73**, 1 (1995).
[45] M. B. Hugenschmidt, L. Gamble, and C. T. Campbell, Surf. Sci. **302**, 329 (1994).
[46] A. Zangwill, *Physics at Surfaces* (Cambridge University Press, Cambridge, 1988).
[47] J. R. MacDonald and J. Barlow, J. Chem. Phys. **39**, 412 (1963).
[48] C. M. Mate, C.-T. Kao, and G. A. Somorjai, Surf. Sci. **206**, 145 (1988).
[49] T. S. Wittrig, D. E. Ibbotson, and W. H. Weinberg, Surf. Sci. **102**, 506 (1981).
[50] K. Bange, R. Döhl, D. E. Grider, and J. K. Sass, Vacuum **33**, 757 (1983).
[51] *CRC Handbook of Chemistry and Physics*, edited by R. D. Linde (CRC Press LLC, Boca Raton, 2000).
[52] B. N. J. Persson and L. H. Dubois, Phys. Rev. B **39**, 8220 (1989).
[53] A. Michaelides, V. A. Ranea, P. L. de Andres, and D. A. King, Phys. Rev. Lett. **90**, 216102 (2003).
[54] C. Zhang and P. J. D. Lindan, J. Chem. Phys. **119**, 9183 (2003).
[55] C. Zhang and P. J. D. Lindan, J. Chem. Phys. **118**, 4620 (2003).
[56] K. Onda, B. Li, and H. Petek (unpublished).